Influence of the flame's secondary reaction zone on a chemiluminescence analysis

Inês Matos Castelão
ines.castelao@tecnico.ulisboa.pt
Instituto Superior Técnico, Universidade de Lisboa, Portugal

July 2017

Abstract

This work focuses on the study of the radical species OH*, CH*, C_2*, as well as CO_2* on premixed methane-air and propane-air Bunsen flames from lean to rich conditions (equivalence ratio values ranging from 0.8 to 1.1). By taking spectroscopic measurements in different axial and radial coordinates of the different flames, applying different methods to extract chemiluminescent signals of the selected excited radicals based on bandhead (type A) or integrated bandwidth (type B) and then reconstructing the signal through three different tomographic methods (Abel, ART and Onion Peeling), with the intention of evaluate how the flame's secondary zone has an impact on the final model of a chemiluminescence analysis. The results have shown i) how variations in the equivalence ratio and the fuel type influence each specie's signal, ii) how tomography affects this type of analysis, and iii) which methods are more adequate (and within which range of equivalence ratio) for a chemiluminescence model.

Keywords: flame chemiluminescence, secondary reaction zone, equivalence ratio sensing, flame tomography, methane, propane.

1. MOTIVATION AND BACKGROUND

Conventional combustion control systems rely on monitoring the CO_2 and/or O_2 content of the exhaust gases, consequently having inherent time-lag efficiency limitations [1]. Other control systems explored for flame control include the use of in-flame solid-state sensors [2], but these suffer erosion due to the harsh thermo-chemical flame environment and may require maintenance or a regular response calibration. Another control system involves the use of optical techniques, in particular flame chemiluminescence, which will be the method used throughout the experimental procedure of this work. Since it is a relatively fast technique with a straightforward implementation, it is a good alternative to the methods listed above, and due to its simplicity and since it may operate away from the extreme combustion conditions (because it isn't an intrusive technique) it has applications not only in active combustion control but also in microgravity experiments [3].

Still, despite the many studies on flame chemiluminescence, basic information on how the two different regions of a premixed laminar flame affect this methodology have yet to be discussed thoroughly in the literature. Previous studies have shown that, in a partially premixed system, combustion occurs in two stages: a primary flame, which is first established, consumes all primary fuel and produces most of the heat release, and a secondary

reaction zone that appears behind the primary flame, when fuel fragments from the rich zones, oxidizer separates from the lean zones and combustion products mix. There is still controversy on whether this last stage can be seen as a diffusion flame and described by diffusion flame models or should be described as distributed combustion [4]. This secondary reaction zone becomes particularly important when applied to the concept of "microflame", which is one of the hot topics in recent combustion studies due to the growing need for portable power generation and the development of microburners [5], microcombustors and micropower devices [6].

Thus, the present work intends to analyze the local chemiluminescence emissions of the excited radicals hydroxyl (OH^*), methylidyne (CH^*) and dicarbon (C_2^*) on these two distinct regions of a laminar premixed flame and consequently evaluate their influence on the chemiluminescent transfer function of the equivalence ratio. The specific excited radicals stated before are preferred not only because they dominate the region between 250 and 600 nm, but also because it is commonly assumed that their emission is primarily chemiluminescent rather than thermal [7, 8, 9].

Throughout the reaction, these highly unstable species tend to change towards a lower state of energy, releasing its energy excess through different channels: one of them in particular is the emission of radiation, whose energy (usually denoted by $h\nu$) corresponds to the transition gap from the initial excited state to a lower state (typically its ground state), which is called chemiluminescence [1]. In order to understand the influence of the secondary reaction zone on the chemiluminescent transfer function, the tracing of spectral signals was made through a pinhole that restricted the line of sight of the spectrometer, and later, the acquired radiation was subjected to tomographic algorithms in order to access the local radiation emissions. This analysis was conducted for three different axial dimensions, for four different equivalence ratios (lean, stoichiometric and rich mixtures) and for premixed air-methane and air-propane mixtures.

In order to determine the equivalence ratio, it is usually used ratios like OH^*/CH^* or C_2^*/CH^* [1, 7, 10], which also attenuate the geometric effects on the signal, caused by the observation area of the optic sensor. Then, it is possible to compare ratios of signals obtained by the spectrometer (raw data) with ratios of the ones already treated with tomographic methods (local data). Afterward, both signals will also be compared with values from other referenced works and the results will allow concluding what is the impact of the secondary zone on the mentioned chemiluminescent signal ratios as well as on the interpretation of the chemiluminescent signals. They will also permit to analyze if there are signal variations throughout the flame, based on the three axial dimensions considered. Moreover, it will also allow evaluating how the type of fuel influences this methodology, since the experimental procedure was repeated for both air-methane and air-propane premixed flames.

2. EXPERIMENTAL PROCEDURE

As stated before, this work carries on the work developed by Trindade [1] and, consequently, the experimental procedure described in this section is largely based on his experimental setup. The goal of the experimental section of this work is to obtain a correlation

between the combustion phenomena in study and the chemiluminescence signal obtained. Thus, the assembly for this work is constituted by three major systems: i) the burner system, ii) the premixture control system, and iii) the chemiluminescence detection system.

The Bunsen burner assembly used on this work was designed by Trindade [1] and was conceived to ensure a steady and fully developed gas flow on laminar regime at the nozzle level. The burner is a circular open nozzle of 20 mm in diameter at the exit, with a high area contraction ratio of $A_{ratio} = 25$ between the entrance and exit section areas. Its aim is to uniformly accelerate the flow, further reducing the flow turbulence and nonuniformities.

The burner setup requires a gas flow control system upstream to ensure the development of stable burning conditions. Air was drawn from the laboratory compressor line after desiccant and filtered operations. The fuels used were bottled research grade methane and propane gases (Alphagaz^{TM}N35, Air Liquide) with a minimum purity of 99.95%. Precision gas flow controllers (Alicat Scientific, Series 16) of 20 and 5 SLPM models were used to separately regulate the air and fuel flow rate selection points. Controllers were operated through FlowVision^{TM}software package that enables individual monitoring of gas flowrate/pressure/temperature during the tests performed.

Flow rate proportions between fuel and air were adjusted according to the equivalence ratio, ϕ, a parameter defined as the ratio between quantities of fuel and air, at actual and stoichiometric proportions. In this work, there were four equivalence ratio conditions analyzed: two lean (0.8 and 0.9), one rich (1.1) and one stoichiometric (1.0).

As mentioned in section 1, a pinhole attached to an optical probe was used in order to restrict the line of the spectrometer. The pinhole's orifice has a diameter of 0.5mm and this assembly has a total length of 147.5mm. Since the aperture of the spectrometer is 0.4mm, it is possible to determine the distance of the assembly to the center of the flame using trigonometry, and choosing a value for the acquired area of flame. In this work, the assembly is at a distance of 115mm and has a projected area on the center of the flame of 1.13mm^2, which means a diameter of 1.2mm.

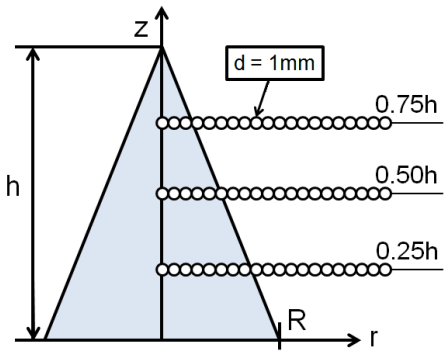

Figure 1: Line of Acquisition

Therefore, for each series, the measurements taken are separated by 1mm, starting from the radial center of the flame to 20mm apart (i.e. r is equal to zero at the center of the flame). As stated in section 1, the measurements will be taken at three different axial dimensions (z equal to 0.25h, 0.5h and 0.75h) as shown in figure 1, that will depend directly on the height of the flame in study.

The signal collection system consists in an optical fiber connected to the spectrometer (QE65000) controlled by SpectraVision^{TM}software running on a personal computer. After the burning system stabilization period, each signal acquisition corresponds to record 10

consecutive spectra with integration time of 30s. Then, each signal is post-processed by a Matlab^{TM}code which removes the background signal and calculates the mean spectrum for each point and the respective deviation, as evidenced by figure 2.

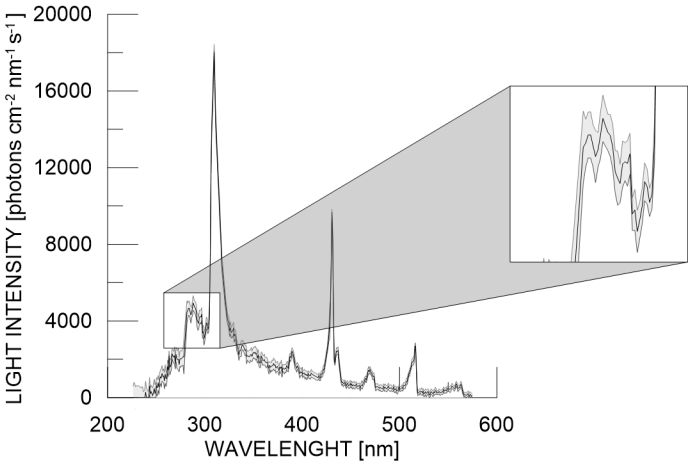

Figure 2: Mean spectrum of a stoichiometric propane flame for r=1mm, z=0.5h

Results are acquired in the range of wavelength from 198.89 to 1000.14 nm, but only further analyzed in the range of 226.24 to 574.61 nm. They are also transformed from the SpectraVision's default units ($\mu W\ nm^{-1} cm^{-2}$) to one that relates with the number of emitted photons ($\#photons\ s^{-1}\ nm^{-1}\ cm^{-2}$).

3. NUMERICAL METHOD

As explained in section 1, the main goal of the present work is to understand the influence of the secondary reaction zone on the chemiluminescent transfer function; consequently, the spectra obtained from the experimental procedure described in the previous section have to be treated in order to be further analyzed.

3.1. Obtaining the signal for each specie

Namely, the first step in this numerical study is to isolate a selected radical signal by filtering contamination, which can be obtained through spectral processing methods which are based on bandhead (peak) [11, 12] or integrated bandwidth (area) [13, 14]; the first method correspond to the maximum intensity signal of a narrow band and the second one is based on the total intensity emitted in a given band (in this work it was considered that the emission bands for OH^*, CH^* and C_2^* range between 275 and 329nm, 379 and 447nm, and 454 and 569nm, respectively).

In this work, there's also a distinction between signals with or without the contribution of the carbon dioxide's continuum: as stated above, in a flame emission spectrum, it is possible to identify several narrow band systems, in which each one is mainly a result of light emissions from characteristic quantum transitions of a specific chemiluminescence radical. Yet, these

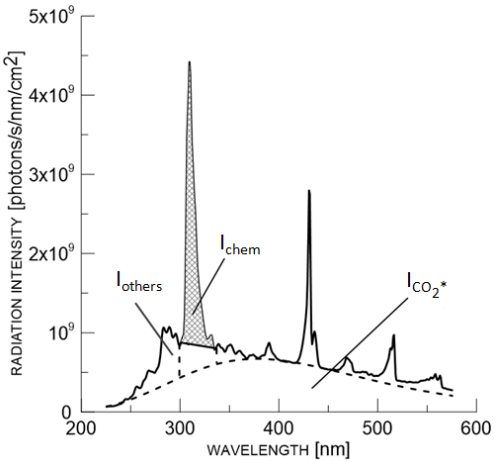

Figure 3: Visual representation of the contribution from different emitters (adapted from [15])

band systems (assigned to those emitters) are superimposed to a broadband continuum, roughly extending from 250 to around 650nm, with no apparent band structure [1].

This continuum radiation is associated with the chemiluminescence from CO_2^* emitters, as a consequence of radiative recombination of CO molecules with atomic oxygen. Therefore, a raw spectral intensity is roughly a sum of three contributions: the chemiluminescence intensity due to the excited radical emissions (I_{chem} in the figure, the one relevant to our analysis), a continuum radiation intensity attributed mainly to the carbon dioxide emitters (I_{CO2*}), and the intensity attributed to other emitters (I_{others}), as evidenced in figure 3.

Several works in the literature [16, 17] have studied CO_2* and tried to create polynomial fits for the broadband continuum. However its broad emission spectrum presents itself as difficulty, making it a challenge to isolate it from other emitters' signal. Therefore, in this work, it was used a numerical method that would search in a neighborhood of predefined values of wavelength for both the inferior and superior limits of the band for each specie, and then would draw a straight line between the two acquired points, thus setting the area that represents the total intensity emitted by the specie's band (shadowed region in figure 3).

Finally, after applying one of the four possible methods (i.e. after calculating the integrated bandwidth or the bandhead for each specie, and after subtracting or keeping the signal associated with CO_2* and other emitters) to the spectrum of every geometric point, it is possible to have four different characteristic signals for each specie with a (ϕ, z, r) defined condition. Thus, it is also possible to obtain a geometrical distribution (i.e. r and z dependent, but independent of the wavelength) for each species, for each flame. Typical geometrical distributions for both OH^* and CH^* (which is also representative of the C_2^* distribution) can be found in the thesis associated with this work [18].

3.2. Reconstructing the signal using tomography

Tomography was first described in a 1953 medical journal's article by B. Pollak [19], which used the technique of planography (another word for tomography) of the chest in cases of

pulmonary tuberculosis. In this work, this method is used to reconstruct the "real" signal of the flame: since it is a hollow flame, the signal recorded by the spectrometer is relative to a small vicinity of points that encompasses the flame front. However, the spectrometer line of sight is approximately a cylinder that will intersect all zones of the flame cone (on both sides) in sight and therefore the radiation intensity calculated for each radial coordinate in subsection 3.1 is actually a superimposition of signals.

Essentially, a tomographic reconstruction or deconvolution is an inverse problem that intends to obtain a discrete estimate of a spatial distribution $I(x, y)$ based on the given projection I_P. Thus, to determine each species' signal at each point, projections of obtained spectroscopic line-of-sight measurements were deconvoluted using tomographic inversion. Three tomographic techniques were investigated, ART [20, 21, 22, 23], Abel [24, 25, 26], and Onion Peeling [26, 27, 28], but only the first one will be further carried out in this work. For a basic 2D object problem like the one explored in this work, we have the following generic equation:

$$I_P = \int I(x, y)\ dA \tag{1}$$

The Algebraic Reconstruction Technique (or ART) is a family of methods for direct reconstruction of three-dimensional objects used in computed tomography that uses iterative algorithms to solve linear equations systems, and was first introduced in 1970 by Gordon, Bender and Herman [20]. Since these methods are iterative, they are more robust in the presence of noise and can successfully incorporate prior information to improve their deconvolutions, and therefore are commonly chosen in most non-medical applications [23].

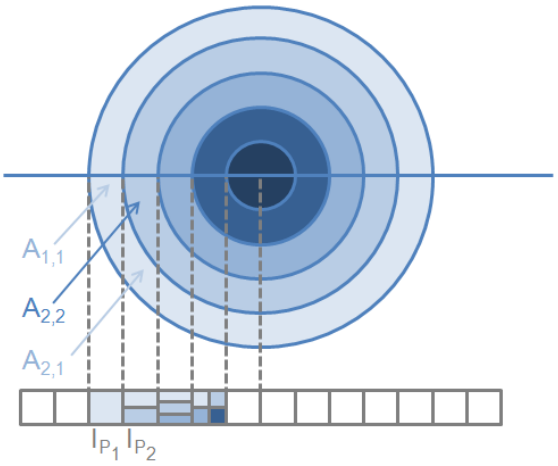

Figure 4: Visual Representation of the ART method

In contrast to methods like the Abel Inversion, ART uses methods entirely based on numerical approximation and on the re-expression of the problem as a system of linear equations, by discretising the projection operator of the equation above; this is achieved by dividing the object volume's domain into a grid of pixels [23]. In this work it is assumed

that the studied object is axisymmetric and as a result the projected intensity I_P is only dependent of r, even though the object's intensity is dependent of x and y - see figure above.

$$\int I_n(x,y)\ dA_{n,n} = I_{Pn} - \sum_{i=1}^{n-1} \int I_i(x,y)\ dA_{n,i} \tag{2}$$

For this reason, the adapted ART method used in this work starts by taking the value obtained for the furthest point from the center of the flame (20 mm, I_{P1} in the figure above), and assign it as a baseline, i.e. the algorithm assumes that I_{P1} is not a superimposition of signals but the direct projection of I_1 (the intensity radiated by the vicinity $A_{1,1}$), and uses geometric formulas to estimate its value. After that, the algorithm takes the next point (19 mm), the projection I_{P2}, and assumes that this value is a direct projection of both I_1 and I_2, thus is able to estimate I_2 by subtracting the value related with I_1 (encountered in the previous step) and applying similar geometric expressions. The method repeats itself until it reaches the center of the flame.

4. RESULTS

After applying the numerical model detailed in the previous chapter on the spectra obtained using the experimental procedure described in section 2, the present chapter intends to display the obtained results which hopefully will permit to draw the conclusions on the influence of the secondary zone on the chemiluminescence transfer function.

As stated before, 4 different methods were used in the scope of this work in order to isolate the signal for each specie, which can be divided into two types: one regarding the choice of band integration vs. band peak (i.e. zero width) - types A and B, respectively -, and the other concerning the subtraction or not of the broadband background radiation - types 1 or 2, respectively. The following figures are representative of the results found and provide a term of comparison between types A and B, while disclosing the influence that the sampling location and the processing methods have in a chemiluminescence analysis. More results can be found in the thesis associated with this work [18].

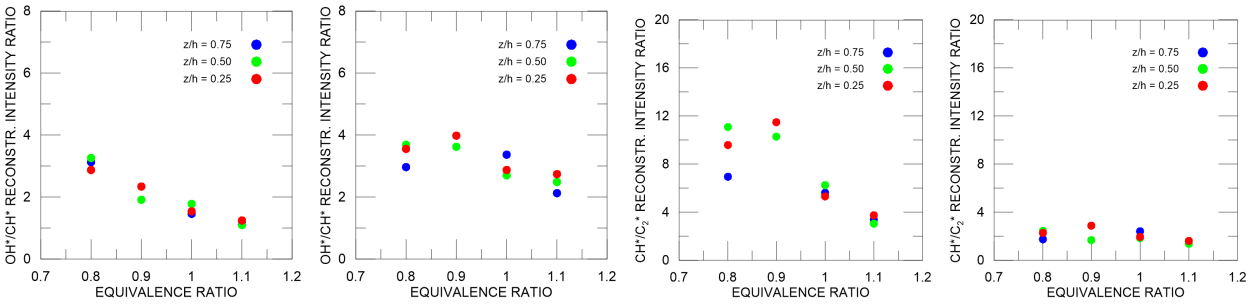

(a) OH*/CH* for A1 (b) OH*/CH* for B1 (c) CH*/C_2^* for A1 (d) CH*/C_2^* for B1

Figure 5: OH*/CH* and CH*/C_2^* ratios vs equivalence ratio

It is possible to observe from sub-figure a) from the figure 5 that for the evaluated range of values for equivalence ratio in this work, the axial sampling location has no influence in

the ratio OH*/CH* with signals showing little to none dispersion of data for the same flame. However, the same result does not apply to the ratio CH*/C_2* (sub-figure c), in which the data dispersion increases towards leaner flames; nonetheless, this outcome doesn't necessarily mean that this method isn't applicable for this specific ratio: for stoichiometric and richer flames, there's little to none influence of the axial sampling location for the same value of equivalence ratio. Furthermore, the dispersion of data for leaner flames can potentially be caused by a numerical error: since the signal from C_2* radicals decreases with the equivalence ratio and this parameter is the denominator of the ratio, it may be originating the dispersion of data.

Unlike the previous method, the method B1 does not have a strictly linear relation between the equivalence ratio and the OH*/CH* reconstructed intensity ratio throughout the studied range for equivalence ratio, showing a maximum for ϕ equal to 0.9 instead of 0.8. This can be justified by the fact that, as stated before, the flame with an equivalence ratio equal to 0.8 had a different volumetric flow rate of propane than the others. Nevertheless, the previous methods showed no signs of being influenced by this circumstance, which could possibly suggest that the method B1 is more fragile to volumetric flow rate variations. The same occurs for the CH*/C_2* ratio even though it's not obvious because of the figure's scale: even though the data are clearly less scattered than the results from the previous methods, the variation amplitude for the same value of equivalence ratio is still relevant, making up to approximately 48 % of the dispersion for the four studied flames. One can hypothesize that the decrease of data dispersion in the CH*/C_2* ratio is related with the contribution of the CO_2* broadband, which has a bigger importance in the B1 method than the A1 (since it is an integration instead of a band peak with zero width), thus overpowering the variations of CH* and C_2 due to changes in equivalence ratio along the flames.

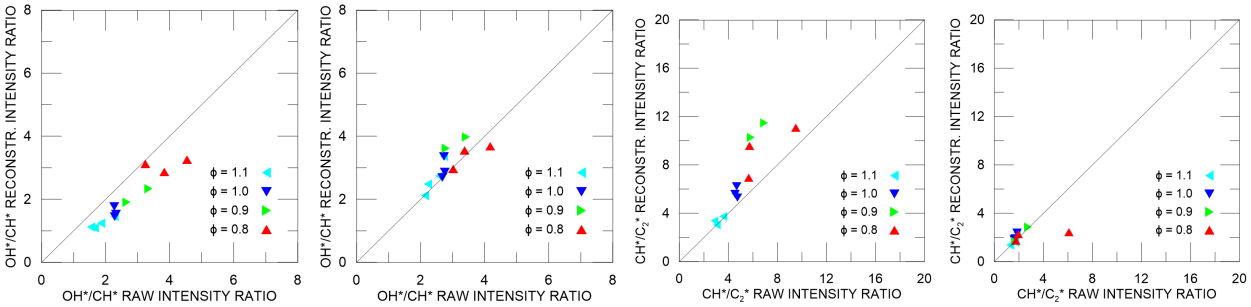

(a) OH*/CH* for A1 (b) OH*/CH* for B1 (c) CH*/C_2^* for A1 (d) CH*/C_2^* for B1

Figure 6: OH*/CH* and CH*/C_2^* reconstructed vs raw ratios

By plotting the intensity ratio before and after the application of the ART technique against each other, i.e. the raw signal taken at the the radial center of the flame (which is comparable to integrate the signal of the whole flame), and the reconstructed signal taken at the flame front's radial coordinate (which is equivalent to take a local measurement in the flame front), it is understand the influence of applying tomography to the data. From the sub-figures a) to c) above, one can observe that there is a clear correlation between the

ratios obtained from reconstructed signals and the ones that use raw signals. Thus, the results suggest that the application of tomographic methods after using the method A1 for both ratios and B1 for OH*/CH* can be considered non-essential.

5. CONCLUSIONS

The present work intended to analyze the impact of the flame's secondary reaction zone on a chemiluminescence model for premixed air-methane and air-propane laminar Bunsen burner flames. In order to achieve this goal, the experimental procedure described in section 2 was performed, focusing on acquiring light intensity data emitted by 8 different flames - 4 values of equivalence ratio (0.8, 0.9, 1, and 1.1) for each fuel type - at 3 different axial coordinates, and 20 different radial coordinates. Then, a numerical model was applied in order to draw conclusions. Spectral data was processed using 4 different methods to extract chemiluminescent signals of the selected excited radicals (OH*, CH* and C_2^*) based on bandhead/peak (type A) or integrated bandwidth/area (type B) and on whether the signals suffer a subtraction of the CO_2^* signal (type 2) or not (type 1). And finally, in order to determine each species' signal at each geometrical point, a tomographic reconstruction ensued: while 3 methods were explored (Abel, ART and Onion Peeling), it was found that only ART modeled appropriately the flame in its entirety.

According to the obtained results, the most robust methods are from type A: A1 and A2 show a clear linear correlation for both ratios and are applicable even without ART (even though A1 is limited to ϕ >0.8), which means that the flame's secondary reaction zone has little to no influence in this type of analysis. For the type B methods, the results aren't quite so robust, specially for B1, which is deemed inadequate for CH*/C_2^* and apparently more fragile to axial location and other parameters variations. B2 holds better correlations than its analogous integral method, having less sensibility to the variations described above in the case of the OH*/CH* ratio, while being applicable for CH*/C_2^* at least for propane flames with ϕ greater than 0.8.

6. References

[1] T. Trindade, *"Chemiluminescence Spectral Identity of Premixed Methane and Propane Flames"*. PhD thesis, Instituto Superior Técnico, 2015.

[2] N. Docquier, S. Candel, *"Combustion control and sensors: a review"*. Progress in Energy and Combustion Sciennce, vol. 28, no. 2, pp: 107-150, 2002.

[3] A. Marchese, F. Dryer, V. Nayagam, R. Colantonio, *"Hydroxyl radical chemiluminescence imaging and the structure of microgravity droplet flames"*. Symposium (International) on Combustion, vol. 26, no. 1, pp: 1219-1226, 1996.

[4] C. Jiménez, B. Cuenot, T. Poinsot, D. Haworth, *"Numerical simulation and modeling for lean stratified propane-air flames"*. Combustion and Flame, vol. 128, no. 1, pp: 1-21, 2002.

[5] D. A. Behrens, I. C. Lee, C. M. Waits, *"Catalytic combustion of alcohols for microburner applications"*. Journal of Power Sources, vol. 195, no. 7, pp: 2008-2013, 2010.

[6] N. S. Kaisarea, D. G. Vlachos, *"A review on microcombustion: Fundamentals, devices and applications"*. Progress in Energy and Combustion Science, vol. 38, no. 3, pp: 321-359, 2012.

[7] A. K. Sandrowitz, J. M. Cooke, N. G. Glumac, *"Flame emission spectroscopy for equivalence ratio monitoring"*. Society for Applied Spectroscopy, vol. 52, no. 5, 1998.

[8] A. G. Gaydon, *"The Spectroscopy of Flames"*. Chapman and Hall, 1974.
[9] R. M. Fristrom. Flame Structure and Processes. Oxford University Press, 1995.
[10] J. Kojima, Y. Ikeda, T. Nakajima, *"Basic aspects of oh(a), ch(a), and c2(d) chemiluminescence in the reaction zone of laminar methaneair premixed flames"*. Combustion and Flame, vol. 140, no. 1-2, pp: 34-35, 2005.
[11] T. Muruganandam, B.H. Kim, M. Morrell, V. Nori, M. Patel, B. Romig, J. Seitzman, *"Optical equivalence ratio sensors for gas turbine combustors"*. Proceedings of the Combustion Institute, vol. 30, no. 1, pp: 1601-1609, 2005.
[12] Y. Hardalupas, M. Orain, C. S. Panoutsos, A. Taylor, J. Olofsson, H. Seyfried, M. Richter, J. Hult, M. Alden, F. Hermann, J. Klingmann, *"Chemiluminescence sensor for local equivalence ratio of reacting mixtures of fuel and air (flameseek)"*. Applied Thermal Engineering, vol. 24, no. 11-12, pp: 1619-1632, 2004.
[13] V. N. Nori, J. M. Seitzman, ' *"Ch(a) - chemiluminescence modeling for combustion diagnostics"*. Proceedings of the Combustion Institute, vol. 32, no. 1, pp: 895-903, 2009.
[14] T. S. Cheng, C.Y. Wu, Y.H. Li, Y.C. Chao, *"Chemiluminescence measurements of local equivalence ratio in a partially premixed flame"*. Combustion Science and Technology, vol. 178, no. 10-11, pp: 1821-1841, 2006.
[15] N. Alves, *"Chemiluminescence analysis of vitiated conditions for methane and propane flames"*. Master thesis, Instituto Superior Técnico, 2016.
[16] M. Kopp, M. Brower, O. Mathieu, E. Petersen, F. Guthe, *"CO2 chemiluminescence study at low and elevated pressures"*. Applied Physics B, vol. 107, no. 3, pp: 529-538, 2012.
[17] J. M. Samaniego, F. N. Egolfopoulos, C. T. Bowman, *"CO2* Chemiluminescence in Premixed Flames"*. Combustion Science and Technology, vol. 109, pp: 183-203, 1995.
[18] I. Castelão, *"Influence of the flame's secondary reaction zone on a chemiluminescence analysis"*. Master thesis, Instituto Superior Técnico, 2017.
[19] B. Pollak, *"Experiences with Planography"*. Chest Journal, vol. 24, no. 6, pp: 663-669, 1953.
[20] R. Gordon, R. Bender, G. T. Herman, *"Algebraic Reconstruction Techniques (ART) for three-dimensional electron microscopy and X-ray photography"*. Journal of Theoretical Biology, vol. 29, no. 3, pp: 476-481, 1970.
[21] R. Marabini, G. T. Herman, J. M. Carazo, *"3D reconstruction in electron microscopy using ART with smooth spherically symmetric volume elements (blobs)"*. Ultramicroscopy, vol. 72, no. 1-2, pp: 53-65, 1998.
[22] N. Oliveira, A. M. Mota, N. Matela, L. Janeiro, P. Almeida, *"Dynamic relaxation in algebraic reconstruction technique (ART) for breast tomosynthesis imaging"*. Computer Methods and Programs in Biomedicine, vol. 132, no. 1, pp: 189-196, 2016.
[23] J. Floyd, *Computed Tomography of Chemiluminescence: A 3D Time Resolved Sensor for Turbulent Combustion*. PhD thesis, Imperial College London, 2009.
[24] N. Abel, *"Auflösung Einer Mechanischen Aufgabe"*. Journal für Die Reine und Angewandte Mathematik, vol. 1, no. 1, pp: 153-157, 1826.
[25] A. Guha, I. M. Schoegl, *"Tomographic Imaging of Flames: Assessment of Reconstruction Error Based on Simulated Results"*. Journal of Propulsion and Power, vol. 30, no.2, pp. 350-359, 2014.
[26] Z. Yuan, S. N. Simonsl, *"The Filtered Abel Transform and Its Application in Combustion Diagnostics"*. Contractor Report NASA/CR2003-212121, National Center for Microgravity Research, 2003.
[27] S. Manzhos, H. Loock, *"Photofragment image analysis using the Onion-Peeling Algorithm"*. Computer Physics Communications, vol. 154, no. 1, pp: 76-87, 2003.
[28] C. J. Dasch, *"One-dimensional tomography: a comparison of Abel, onion-peeling, and filtered backprojection methods"*. Applied Optics, vol. 31, no. 8, pp. 1146, 1992.
[29] T. García-Armingol, Y. Hardalupas, A.M.K.P. Taylor, J. Ballester, *"Effect of local flame properties on chemiluminescence-based stoichiometry measurement"*. Experimental Thermal and Fluid Science, vol. 53, no. 1, pp 93-103, 2014.